ESA CONTRACT REPORT

Contract Report to the European Space Agency

Milestone 1 Tech Note - Part 1: SMOS Global Surface Emission Model

Patricia de Rosnay, Matthias Drusch and Joaquín Muñoz Sabater

Progress report for ESA contract 3-11640/06/I-LG

European Centre for Medium-Range Weather Forecasts
Europäisches Zentrum für mittelfristige Wettervorhersage
Centre européen pour les prévisions météorologiques à moyen terme

ECMWF

Series: ECMWF ESA Project Report Series

A full list of ECMWF Publications can be found on our web site under:
http://www.ecmwf.int/publications/

Contact: library@ecmwf.int

European Centre for Medium Range Weather Forecasts
Shinfield Park, Reading, RG2 9AX, England

Contract Report to the European Space Agency

Milestone 1 Tech Note - Part 1: SMOS Global Surface Emission Model

Authors: Patricia de Rosnay, Matthias Drusch[1] *and Joaquín Muñoz Sabater*

Progress report for ESA contract 3-11640/06/I-LG

[1] Now at ESA/ESTEC, Noordwijk, The Netherland

European Centre for Medium-Range Weather Forecasts
Shinfield Park, Reading, Berkshire, UK

November 2009

Contents

	Name	Company
First version prepared by (October 2009)	P. de Rosnay M. Drusch J. Muñoz Sabater	ECMWF ESA/ESTEC ECMWF
Quality Visa	E. Källén	ECMWF
Application Authorized by	N. Wright	ESA/ESRIN

Distribution list:

ESA/ESRIN
Luc Govaert
Susanne Mecklenburg
Norrie Wright
ESA ESRIN Documentation Desk

SERCO
Raffaele Crapolicchio

ESA/ESTEC
Catherine Bouzinac
Steven Delwart
Matthias Drusch

ECMWF
HR
OD and RD Division and Section Heads

Abstract

Contracted by the European Space Agency (ESA), the European Centre for Medium-Range Weather Forecasts (ECMWF) is involved in global monitoring and data assimilation of the Soil Moisture and Ocean Salinity (SMOS) mission data. To this end the Community Microwave Emission Model (CMEM) has been developed by ECMWF as the forward operator for low frequency passive microwave brightness temperatures (from 1GHz to 20 GHz) of the surface. CMEM is a new highly modular software package providing input/output interfaces for the Numerical Weather Prediction Community. CMEM's physics is based on the parameterizations used in the L-Band Microwave Emission of the Biosphere and Land Surface Microwave Emission Model. CMEM modularity allows considering different parameterizations of the soil dielectric constant as well as different soil approaches (either coherent of incoherent) and different effective temperature, roughness, vegetation and atmospheric contribution opacity models. This report is Part 1 of the first Milestone Technical Note / Progress Report of the ESA Request for Quotation RfQ 3-11640/06/I-LG. It provides a scientific and technical documentation of CMEM.

1 Introduction

SMOS (Soil Moisture and Ocean Salinity) is the first mission specifically devoted to remote sensing of soil moisture over land (Kerr, 2007; Kerr et al., 2001). The mission provides interferometric measurements of multi-angular, bi-polarised brightness temperatures at L-band in near-real time. ECMWF plays a major role in preparing the use of SMOS brightness temperatures by the Numerical Weather Prediction (NWP) community. ECMWF's contribution to the SMOS mission is two-fold: first, a data monitoring system for the SMOS near real time product is being developed to provide a timely quality check for ESA and the SMOS calibration and validation teams. Second, SMOS brightness temperature data will be assimilated over land surfaces in ECMWF's global NWP system to quantify the impact of this new observation type on forecast quality.
One main component of the monitoring and of the surface data assimilation system is the observation operator that transforms model fields (soil moisture and ocean salinity) into observation space (brightness temperatures). In the context of this ESA contract the Community Microwave Emission Model (CMEM) has been developed by ECMWF as the forward operator for low-frequency passive microwave brightness temperatures at 1 to 20 GHz. CMEM is a modular code that includes a choice of several parameterisations including those used in the ESA level 2 processor. CMEM is one of the ESA SMOS tools and it is available to the entire community through the ECMWF web pages: http://www.ecmwf.int/research/ESA_projects/SMOS/cmem/cmem_index.html.

This report provides a scientific and technical documentation on the global emissivity model CMEM. It is produced as Part 1 of the first Milestone Technical Note / Progress Report [MS1TN-P1] and it is complementary from the MS1TN-P2 which describes the IFS implementation. The following section shortly describes CMEM's implementation strategy. Section 3 provides a description of CMEM's modular parameterisations. In section 4 results of three scientific studies are presented. These results, published in peer reviewed journals, provide quantitative results on CMEM calibration and intercomparison studies conducted at several frequencies and at several spatial and temporal scales. Section 5 gives a technical description of CMEM and section 6 concludes.

2 Implementation strategy

Operational numerical weather forecast systems are widely used to evaluate and analyse new types of satellite observations. Numerical weather prediction (NWP) centres are prime customers as observations are used in the

analyses to derive level 2 retrieved geophysical parameters (eg soil moisture or ocean salinity for SMOS) from the observed brightness temperatures or radiances.

Before the SMOS launch, forecast systems could be used in the product definition phase. Based on modeled atmospheric and land state variables, the effect of different parameterizations and auxiliary data sets on the simulated brightness temperatures has been analysed.

After the SMOS launch, when real SMOS observations are available, monitoring, i.e. comparison between the modeled equivalent of the observation and the observation itself, makes a significant contribution to the calibration / validation activities. Any systematic error or spikes, become visible and can be reported to ESA and the other calibration and validation teams without significant delays.

In this context, CMEM implementation strategy includes the development and implementation of the CMEM forward model for SMOS level 1 data at ECMWF for quality monitoring and the development of the assimilation scheme for SMOS level 1c brightness temperature in ECMWF's global NWP system.

For the atmospheric radiative transfer calculations, the RTTOV [Radiative Transfer model for Television Infrared Orbiting Satellite (TIROS) Operational Vertical Sounder (TOVS)] software package has been developed as a community model. It is updated and maintained by the UK Met Office under the framework of EUMETSAT's NWP Satellite Application Facility (SAF). RTTOV is used in the ECMWF IFS for atmospheric radiative transfer computation. Although CMEM has been designed for frequencies below 20 GHz, its modular structure allows upgrades to higher frequencies and CMEM is being interfaced to the RTTOV software package.

3 CMEM physics

3.1 Radiative transfer equations

The physics of CMEM is based on a simplified solution of the vector radiative transfer equation. It comprises parameterisations used in the L-Band Microwave Emission of the Biosphere model (L-MEB, Wigneron et al., 2007) and the Land Surface Microwave Emission Model (LSMEM, Drusch et al., 2001). CMEM's modularity allows different parameterisations to be considered for the main components. Although CMEM has been designed for frequencies below 20 GHz, its modular structure allows future upgrades to higher frequencies and applications in the atmospheric 4D-Var analysis system.
For polarisation p the brightness temperature over snow free areas at the top of the atmosphere $T_{Btoa,p}$ can be expressed as:

$$T_{Btoa,p} = T_{Bau,p} + exp(-\tau_{atm,p}) \cdot T_{Btov,p} \quad (1)$$

and

$$\begin{aligned} T_{Btov,p} &= T_{Bsoil,p} \cdot exp(-\tau_{veg,p}) \\ &+ T_{Bveg,p}(1 + r_{r,p} \cdot exp(-\tau_{veg,p})) \\ &+ T_{Bad,p} \cdot r_{r,p} \cdot exp(-2 \cdot \tau_{veg,p}) \end{aligned} \quad (2)$$

where $T_{Bau,p}$ (K) is the up-welling atmospheric emission and $\tau_{atm,p}$ is the atmospheric optical depth. $T_{Btov,p}$ (K) is the top of vegetation brightness temperature when the vegetation is represented as a single-scattering layer above a rough surface. $T_{Bsoil,p}$ (K), $T_{Bveg,p}$ (K) and $T_{Bad,p}$ (K) are the soil, vegetation layer and downward atmospheric contributions, respectively. $r_{r,p}$ is the soil reflectivity of the rough surface (one minus the emissivity $e_{r,p}$) and $\tau_{veg,p}$ is the vegetation optical depth along the viewing path. The contribution emitted from the soil can be written as the product of the soil emissivity $e_{r,p}$ and the effective temperature:

$$T_{Bsoil,p} = T_{eff} \cdot e_{r,p} \quad (3)$$

Open water surfaces (i.e. lakes, rivers) represents a challenge for soil moisture retrievals as well as for data assimilation applications. For the future soil moisture analysis, observations with open water fractions exceeding 5 % will be flagged and excluded. In CMEM skin temperature is used as a proxy for lake and sea effective temperature. The salinity of open water in a land pixel is set to 0 psu. For sea pixels the salinity is obtained either from the ocean analysis (when CMEM is in the IFS, see the Sea Surface Salinity technical note) or set to a constant value (32.5 psu) for offline use of CMEM. In CMEM the Klein and Swift (1977) parameterisation for the dielectric constant of flat water surfaces of saline water is used over both lakes and ocean surfaces. For future SMOS monitoring activities, the forward model used in the level 2 processor for ocean salinity (L2OS) will be used over ocean surfaces, allowing to account for surface roughness and galactic noise contributions, as well as for faraday rotation, that can have large effects on Sea surface emission. It is currently being externalised from the processor by ARGANS in order to be used at ECMWF for SMOS monitoring over ocean surface. For copyright reasons, the ocean emission model will be interfaced with CMEM rather than being implemented in CMEM and it will be possible to use CMEM with or without the ocean emission model.

CMEM comprises four modules for the computation of the contributions from soil, vegetation, snow and the atmosphere, respectively. The code is designed to be highly modular and for each microwave modelling component, a choice of several parameterisations are considered. Table 1 summarises the modular structure of CMEM and lists for each module the choice of modelling options considered. The choice of parameterizations proposed in the soil module and in the vegetation module are described hereafter.

Module	Variable	Parameterisations		
Soil	ε	Wang & Schmugge (1980)	Dobson et al. (1985)	Mironov et al. (2004)
	T_{eff}	Choudhury et al. (1982)	Holmes et al. (2006)	Wigneron et al. (2001)
		T_{surf}		
	$e_{s,p}$	Fresnel law	Wilheit (1978)	
	$e_{r,p}$	Choudhury et al. (1979)	Wigneron et al. (2001)	SMOS ATBD (2007)
		Wegmüller & Mätzler (1999)	Wigneron et al. (2007)	
Veg.	$\tau_{veg,p}$	Wegmüller et al. (1995)	Wigneron et al. (2007)	Kirdyashev et al. (1979)
		Jackson and O'Neill (1990)		
Snow	rsn_p	Pulliainen et al. (1999)		
Atm.	$\tau_{atm,p}$	Pellarin et al. (2002)	Liebe (2004)	Ulaby et al. (1986)

Table 1: Modular configuration of CMEM. For each component, the key variable is indicated and the list of options is provided. The soil module includes 4 components: the dielectric mixing model (ε), the effective temperature model (T_{eff}), the smooth surface emissivity model ($e_{s,p}$), the rough surface emissivity, $e_{r,p}$. For each of them several parameterisations are proposed. The vegetation module key variable is the vegetation optical thickness $\tau_{veg,p}$. The snow module computes the snow reflectivity rsn_p. The atmospheric module provides the atmosphere optical thickness $\tau_{atm,p}$.

3.2 Soil module

The soil module of CMEM includes four components to compute the soil dielectric constant ε, the effective temperature T_{eff}, smooth soil emissivity $e_{s,p}$ and rough soil emissivity $e_{r,p}$.

Based on the Rayleigh-Jeans approximation for the microwave domain the soil brightness temperature is expressed as the product of the soil emissivity $e_{r,p}$ and the effective temperature ($T_{Bsoil,p} = T_{eff} \cdot e_{r,p}$).

3.2.1 Dielectric mixing model

Microwave remote sensing of soil moisture relies on the large contrast between the dielectric constant of water (~ 80)and that of dry soils (~ 4). The soil dielectric mixing model computes the soil dielectric constant ε as a function of volumetric soil moisture (θ), soil texture, frequency of detection and surface soil temperature T_{surf}. It is an essential part of forward modelling and retrieval approaches. Three semi-empirical dielectric models are available through CMEM: Mironov et al. (2004), Dobson et al. (1985) and Wang & Schmugge (1980). The Wang and Schmugge model and the Mironov model consider the effect of bound water on the dielectric constant. They are limited to rather short frequencies of 1-5 GHz and 1-10 GHz, respectively. The Dobson model is valid for a larger range of frequency (1-18 GHz), but the dielectric constants computed from the Wang & Schmugge (1980) and the Mironov et al. (2004) models are in better agreement with measurements for a large range of soil texture types (Cardona et al., 2005; Mironov et al., 2004).

3.2.2 Smooth emissivity model

The soil emissivity model describes the relationship between soil emissivity and soil dielectric constant. For a smooth surface the Fresnel equation is commonly used in microwave emission models to compute the air-soil interface reflectivity. The Wilheit (1978) model is more physically based and accounts for both coherent and incoherent components of the signal. It represents the soil as a stratified medium where the soil dielectric constant and temperature vertical profiles are used to compute the resulting air-soil interface emission.

3.2.3 Soil roughness model

Rough surfaces are characterized by higher emissivities. In addition, the difference between horizontally and vertically polarized brightness temperatures is reduced.
Wang and Choudhury (1981) proposed a semi-empirical approach to represent soil roughness effects on the microwave emission. The rough emissivity is computed as a function of the smooth emissivity and three parameters Q, h, N:

$$r_{r,p} = (Q \cdot r_{s,p} + (1-Q) \cdot r_{s,q}) \cdot exp\left(-h \cdot cos^N \psi\right) \tag{4}$$

where p and q refer to the polarization states, Q is the polarization mixing factor, N describes the angular dependence, h is the roughness parameter and ψ the incidence angle. The mixing factor Q is considered to be very low at low frequencies and is generally set to 0 (Wigneron et al., 2007; Njoku et al., 2003). Based on equation 4 two parameterizations have been proposed with $N = 0$ and the following computation for the h parameter:

$$h = (2k\sigma)^2 \ (Choudhury\,et\,al., 1979) \tag{5}$$

$$h = 1.3972 \cdot (s/L_c)^{0.5879} \ (Wigneron\,et\,al., 2001) \tag{6}$$

where k is the wave number and L and σ are correlation length and standard deviation of surface roughness. In Wigneron et al. (2001), the slope parameter $m = s/L_c$ is used as a calibration parameter in equation 6. The global scale study conducted by Pellarin et al. (2002) used the Wigneron et al. (2001) parameterization, with a constant value of $L = 6.0$cm, $\sigma = 0.44$cm, leading to $h = 0.3$. However, a more recent soil roughness parameterization has been developed and validated against field experiments. It is based on equation 4 and accounts for the dependency of the roughness parameter on soil moisture and soil texture (SMOS ATBD, 2007).

In addition, the roughness parameter can be computed as a function of both soil moisture and vegetation type with N depending on vegetation and polarization (Wigneron et al., 2007). Wegmüller & Mätzler (1999) proposed a different approach based on horizontal smooth emissivity with a single roughness parameter $h = k \cdot \sigma$.

3.2.4 *Effective soil temperature model*

A simple parameterization of the effective temperature was first proposed by Choudhury et al. (1982):

$$T_{eff} = T_{deep} - (T_{deep} - T_{surf}) \cdot C \tag{7}$$

with T_{deep} and T_{surf} the soil temperature at depth (at $\sim$ 50 cm) and surface soil temperature (at $\sim$ 5 cm) and C an empirical parameter which depends on frequency. This parameterization was modified by Wigneron et al. (2001) for L-band radiometry including a dependency of C to soil moisture: and coefficients b and w0: $C(\theta) = (\theta/w0)^b$. Holmes et al. (2006) proposed a more complex parameterization where C is expressed as a function of the dielectric constant. Based on the long term SMOSREX data set, de Rosnay et al. (2006) provide an inter-comparison of these three parameterizations.

3.3 Vegetation module

In CMEM vegetation is represented through $\tau - \omega$ approaches: The vegetation layer has a direct contributions to the TOA signal and attenuates the emission from the underlying soil:

$$T_{Bveg,p} = T_c \cdot (1 - \omega_p) \cdot (1 - exp(-\tau_{veg,p})) \tag{8}$$

where T_c is the canopy temperature and ω_p is the single scattering albedo at polarization p. Based on equation 8, Jackson and Schmugge (1991) proposed a simple parameterization to compute the vegetation optical thickness:

$$\tau_{veg,p} = b \cdot \frac{VWC}{cos\psi} \tag{9}$$

where b and VWC are the vegetation structure parameter and the vegetation water content, respectively. For the high vegetation types rain forest, deciduous forest and coniferous forest the VWC is set to values of $6kg/m^2$, $4kg/m^2$, $3kg/m^2$, respectively, following Pellarin et al. (2002). VWC is described as a function of Leaf Area Index (LAI) for low vegetation types (grass and crops):

$$VWC = 0.5 \cdot LAI \tag{10}$$

The default values for the b parameter are 0.2 and 0.15 for grass and crops, and 0.33 for forests. The single scattering albedo is constant at $\omega = 0.05$ for low vegetation types (grass and crops) and $\omega = 0.15$ for high vegetation types (forests). However, these values can be changes through the CMEM input data files.

The Wigneron et al. (2007) vegetation optical thickness model also describes the vegetation effect with equation 8. In their formulation the single scattering albedo depends on vegetation type and polarization. The polarized optical thickness is expressed as:

$$\tau_{veg,p} = \tau_{nadir} \cdot (cos^2\psi + tt_p sin^2\psi) \frac{1}{cos\psi} \tag{11}$$

$$\tau_{nadir} = b^{'} \cdot LAI + b^{''} \tag{12}$$

where tt_p parameters represent the angular effect on vegetation optical thickness for each polarization and vegetation types. τ_{nadir} is the nadir optical depth and $b^{'}$, $b^{''}$ are the vegetation structure parameters.

The Kirdyashev et al. (1979) parameterization expresses the vegetation optical thichness as a function of the wave number k (between 1 GHz and 7.5GHz), the dielectric constant of saline water, ε''_{sw} (imaginary part), VWC, indidence angle ψ, water density ρ_{water} and a vegetation structure parameter a_{geo}:

$$\tau_{veg,p} = a_{geo} \cdot k \cdot \frac{VWC}{\rho_{water}} \cdot \varepsilon''_{sw} \cdot \frac{1}{cos\psi} \tag{13}$$

This parameterization was extended to a larger range of frequencies (1-100 GHz) by Wegmüller et al. (1995).

3.4 Sub-grid scale representation of vegetation

$T_{Btov,p}$ (equation 2) can be computed for each model grid box taking the sub-grid scale variability of the land surface into account. Up to seven tiles can be considered in each CMEM grid box: bare soil, low vegetation, high vegetation (each are either free of snow or snow-covered, and open water. For low and high vegetation tiles, the dominant type is determined from the land cover data base. For each grid cell, brightness temperatures are computed separately for each tile. The grid cell averaged brightness temperature is computed using the weighted sum of each tile.

The brightness temperature at the top of the vegetation ($T_{Btov,p}$, Equation 2) can be computed for each model grid box taking the sub-grid scale variability of the land surface into account. Up to seven tiles can be considered in each CMEM grid box: bare soil, low vegetation, high vegetation (each are either free of snow or snow-covered) and open water. For low and high vegetation tiles, the dominant type is determined from the land-cover data base. For each grid cell, brightness temperatures are computed separately for each tile. The grid-cell averaged brightness temperature is computed using the weighted sum of each tile.

4 Microwave emission models intercomparison

Several studies have been conducted at ECMWF with CMEM to simulate, calibrate and evaluate the computed brightness temperature at different spatial and temporal scales (Drusch et al., 2008; de Rosnay et al., 2009; Sabater et al., 2009). Different observing configuration (L-band, C-band, X-band) at several incidence angles have been considered and evaluated as well as different forward modelling approaches. These results are summarised hereafter. They provide quantitative assessment of the observation minus model departures and help identify the optimal forward-model configuration to be used for SMOS activities in NWP.

4.1 CMEM calibration using Skylab observations

The NASA Skylab mission in 1973-1974 was the first to provide L-band (1.4 GHz) satellite measurements from its S-194 instruments. It performed nadir measurements at a ground resolution of about 110 km (Eagleman and Lin, 1976). Although the observation data set is limited to nine overpasses between June 1973 and January 1974 it is currently the only existing space-borne L-band data set available (Jackson et al., 2004). Moreover, the observations cover a wide range of climates and a variety of biomes.
A calibration study has been conducted by comparing ERA-40 (ECMWF's 40-year climate re-analysis, Uppala and co authors , 2005) based L-band brightness temperatures with the Skylab observations at L-band (Drusch et al., 2008). CMEM input data comprise surface fields from ERA-40, vegetation data from the ECOCLIMAP data set (Masson et al., 2003), and the Food and Agriculture Organization (FAO) soil data base (FAO, 2003). Figure 1 indicates the SKYLAB overpasses and observation dates.

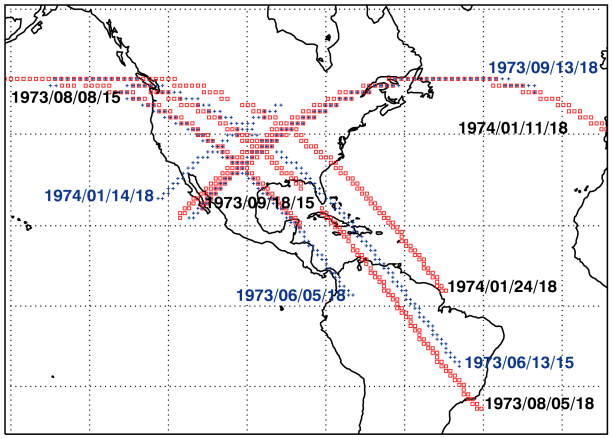

Figure 1: SKYLAB observations at L-band and corresponding data and time (UTC). Blue symbols indicate overpasses for which the data were used for the calibration of CMEM. Validation was performed for data acquired on overpasses indicated in red.

In a first step, different parameterisations for surface roughness and the vegetation optical depth were used to provide an estimate on the corresponding brightness temperature sensitivities. Then the radiometric surface roughness, which has to be estimated and does not feed back to the NWP model, was adjusted to provide bias free estimates. In total, ten combinations of different roughness and vegetation parameterisations were used to compute brightness temperatures. For these computations the recommended parameter values from the reviewed literature have been adopted. They are performed to gauge the range output values and determine sensitivities. Figure 2a,b shows our reference configuration using parameterisations that have often been applied in the literature.
A second configuration gave promising results when data from field experiments were used (Wigneron et al., 2007). However, in combination with the ECMWF model fields and the NWP auxiliary data sets the systematic and random errors were comparably large. For North America we obtain a correlation coefficient of 0.04 and a bias of 23.1 K (Figure 2c). The corresponding values for the South American data are 0.58 and 27.9 K (Figure 2d). The best results for both continents have been obtained using Wigneron et al. (2001) to describe the effects of surface roughness and Kirdyashev et al. (1979) for the parameterisation of vegetation (Figure 2e,f).

The main results from the calibration study Drusch et al. (2008) are:

- Calibrating CMEM results in low biases, which are acceptable for data assimilation applications.
- The rather large RMS errors over North America are caused by errors in the ERA-40 soil moisture fields.
- Systematic differences in the dynamic range of the modelled and observed brightness temperatures are an artefact of the NWP model parameters, which define TESSEL's soil moisture climatology.
- These differences can not be reduced in the calibration process but should be corrected through a statistical correction method.

4.2 The SMOSREX field experiment

The SMOSREX (Soil Monitoring Of the Soil Reservoir EXperiment) field experiment site is located near Toulouse, France. For this location a continuous data set from 2003 to 2008 is available comprising in-situ measurements of soil moisture, soil temperature, meteorological variables and multi-angular highly accurate L-band observations (de Rosnay et al., 2006).

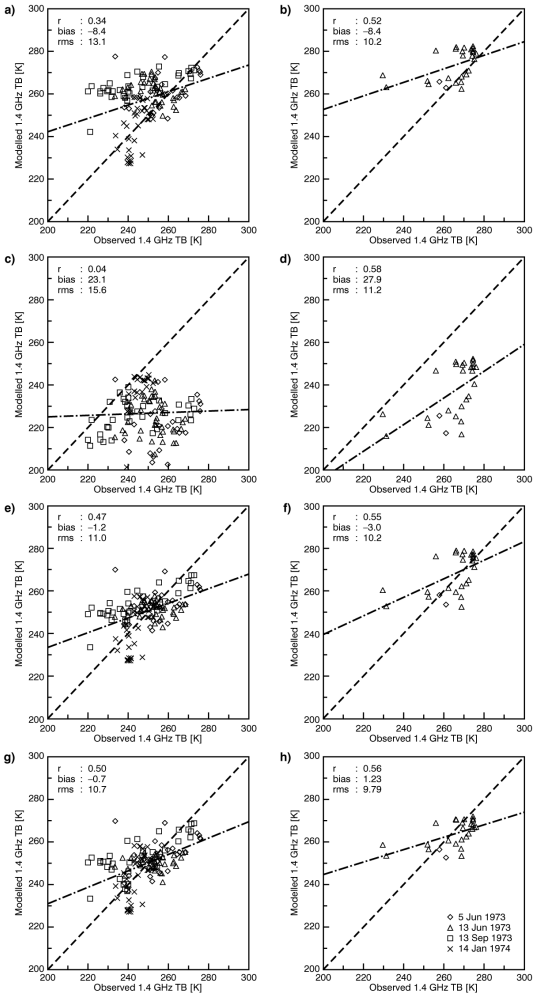

Figure 2: Calibration of the ERA-40 based CMEM simulation at L-band for the SKYLAB overpasses over North America (left) and South America (right). The top panel (a,b) considers the Wigneron et al. (2001) and Jackson and Schmugge (1991) parameterisations for the soil roughness and vegetation optical thickness respectively. The results of the second panel (c,d) are obtained using the parameterisations of Wigneron et al. (2007) for both. Third and fourth panels (e,f,g,h) results are for the Wigneron et al. (2001) soil roughness and the Kirdyashev et al. (1979) vegetation optical thickness, considering different values of the parameters. The dashed-dotted line is the linear regression.

Sensitivity studies have been conducted for different incidence angles and different CMEM configurations using (i) the observed data and (ii) output from ECMWF's operational NWP model (Sabater et al., 2009). In both cases modelled brightness temperatures have been compared against the L-band observations. Here we focus on results obtained using the ECMWF model (with HTESSEL) at T799 spectral resolution. The comparison is based on data for 2004 and we use four statistical indices to assess the quality of the simulations: bias, root mean square error (RMSE), relative explained variance (R^2), and the Nash coefficient.

Figure 3 summarises the comparison between modelled and observed brightness temperatures at vertical polarisation. The statistical indices obtained for two different model configurations are presented as a function of incidence angle. For Wigneron's parameterisation of vegetation optical depth the lowest bias is obtained for an incidence angle of $40^c irc$. The R^2 values indicate that the temporal dynamics are well captured by the ECMWF synthetic brightness temperatures at any incidence angle, although best correlation ($R^2 = 0.82$) is obtained at 50°. RMSE in simulated brightness temperature increases with the incidence angle and the Nash coefficient suggests the best result for an observing angle of 30°.

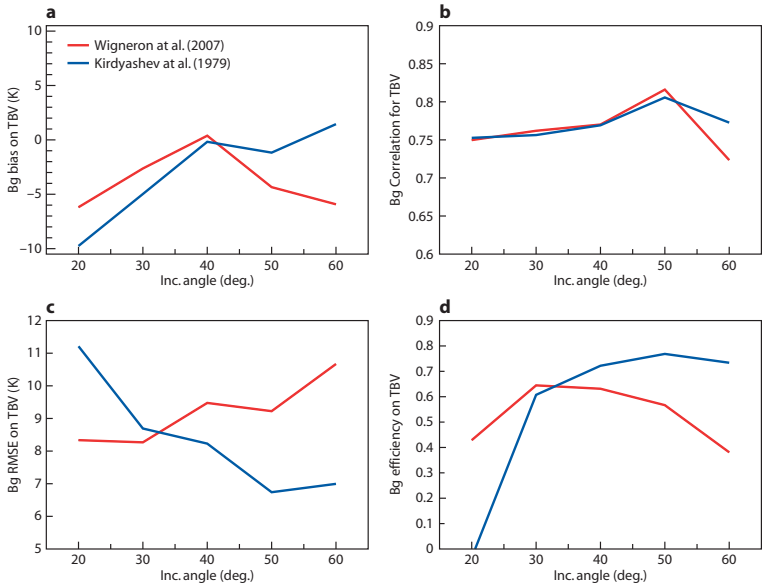

Figure 3: Background error of the ECMWF synthetic brightness temperature (K) over the SMOSREX pixel, as a function of the incidence angle, at vertical polarisation for two different microwave modelling approaches of the vegetation optical depth by Wigneron et al. (2007) and Kirdyashev et al. (1979) (see in Table 1). The top panel shows the bias (left) and the correlation coefficient R^2 (right). The bottom panel shows the RMSE (left) and the Nash coefficient (right).

When the Kirdyashev model is used in the forward operator better performances are obtained for incidence angles of 40 to 60° than for lower angles. Overall, the best modelling/observing configuration is obtained when the Kirdyashev opacity model is used for an observing angle of 50°. The results also suggest that a future bias correction scheme for SMOS should depend on the viewing angle. The good agreement with R^2 values exceeding 0.7 at vertical polarisation is particularly encouraging, since it applies to both parameterisations and all angles used. We have thus shown that the coupled IFS / CMEM system can capture the main variability on the point scale.

4.3 The ALMIP inter-comparison of microwave emission models

A large-scale CMEM evaluation study for low frequency passive microwave has been conducted at C-band, using the AMSR-E data over West Africa (de Rosnay et al., 2009). This work has been conducted with an ensemble of Land Surface Models (LSMs) in the joint framework of the SMOS and the ALMIP (AMMA Land Surface Model Intercomparison Project) projects (Boone et al. , 2009). ALMIP is a coordinated land surface modelling activity conducted within the AMMA project. One of its objectives is to address the contribution of soil moisture dynamics to the African monsoon dynamics and variability (Redelsperger et al., 2006).

The Advanced Microwave Scanning Radiometer on Earth Observing System (AMSR-E) on the NASA's AQUA satellite was launched in 2002 and it is still operating. AMSR-E measures microwave brightness temperatures at five frequencies, including C-band and X-band channels (6.9 and 10.7 GHz), with a ground resolution of about 60 km at C-band for an incidence angle of 55° (Njoku et al., 2003). AMSR-E products include brightness temperature as well as soil moisture and vegetation water content products. They are archived and distributed routinely by the NASA National Snow and Ice Data Center's (NSIDC) Distributed Active Archive Center (DAAC) (Njoku, 2004).

In the recently completed phase-1 of ALMIP, an ensemble of state-of-the-art LSMs have been run offline (i.e. decoupled from an atmospheric model) at a regional scale over West Africa for five annual cycles (2002 to

2006). Eleven LSMs participated in the inter-comparison (Boone et al. , 2009). For ALMIP-MEM (de Rosnay et al., 2009) the eight LSMs that are used for NWP applications were coupled with CMEM (Table 2). All participating LSMs require the following input forcing fields: precipitation, short-wave and long-wave radiative fluxes, wind speed and direction, 2m air humidity and temperature and surface pressure.

For each LSM, two ALMIP experiments were conducted with different precipitation and radiative-flux forcing. In the control experiment (EXP1), the LSMs were forced with the ECMWF forecasts for 2002-2006. In the second experiment (EXP2), ECMWF fields are hybridised with the satellite based precipitation products obtained in EPSAT-SG (Estimation des Pluies par SATellite - Seconde Génération, (Chopin et al., 2004)) and the OSI-SAF (Ocean and Sea-Ice - Satellite Application Facility) radiative fluxes. Boone and de Rosnay (2007) have shown that the hybridised forcing data set used in EXP2 is more realistic. In particular, the extension of the African monsoon to the north is better represented than in the ECMWF model precipitation which underestimates rainfall occurrence and intensity over the Sahel.

Name	Group	Reference
ISBA-FR	CNRM/Météo-France	Noilhan and Planton (1989)
ISBA-DF	CNRM/Météo-France	Boone et al. (2000)
HTESSEL	ECMWF	Balsamo et al. (2008)
TESSEL	ECMWF	Viterbo and Beljaars (1995)
CTESSEL	ECMWF	Jarlan et al. (2007)
JULES	MetOffice	Blyth et al. (2006)
NOAH	NCEP/EMC	Chen and Dudhia (2001)
ORCHIDEE-CWRR	IPSL	de Rosnay et al. (2002)

Table 2: Land Surface Models used for ALMIP-MEM.

Both EXP1 and EXP2 were performed at a 0.5° resolution over the West African domain (from 5°S to 20°N and from 20°W to 30°E). ALMIP outputs have been provided for each ALMIP LSM at a 3 hour time step. They include soil moisture and soil temperature profiles, runoff, sensible and latent heat fluxes. Table 3 summarises the different microwave modelling options tested in ALMIP-MEM.

Figure 4 shows the spatial distributions of observed (AMSR-E) and simulated (ORCHIDEE / CMEM) brightness temperatures at horizontal polarisation on days 200-201 of 2006. The data represent the descending orbit and are based on the configuration using the Mironov model to simulate the dielectric constant and the Kirdyashev parameterisation for the vegetation optical thickness. High values of soil moisture result in low emissions and thus in low brightness temperatures. In contrast, areas with high vegetation water content, as encountered at latitude between 4°S and 10°N, have high brightness temperature values. This figure clearly shows the presence of a wet patch centred on 2°W, 15°N in the Sahel region. This typically corresponds to the occurrence of a monsoon season meso-scale convective rainfall event. This wet patch is well captured by the EXP2 ALMIP-MEM simulation. However, it is not captured in EXP1 for which the ECMWF precipitation forcing data have

	Dielectric constant		
Vegetation optical depth	Dobson et al. (1985)	Mironov et al. (2004)	Wang and Schmugge (1980)
Jackson and O'Neill (1990)	1	5	9
Kirdyashev et al.(1979)	2	6	10
Wegmüller et al., (1995)	3	7	11
Wigneron et al. (2007)	4	8	12

Table 3: Physical parameterizations used in CMEM for ALMIP-MEM. Twelve configurations are considered for different combination of soil dielectric and vegetation optical depth models.

been used. It is clear from this figure that the errors in simulated brightness temperatures will be highly dependent on forecast errors in precipitation. In turn, these results suggest that low-frequency passive microwave observations can detect errors introduced through uncertainties in the precipitation forcing. Figure 5 represents

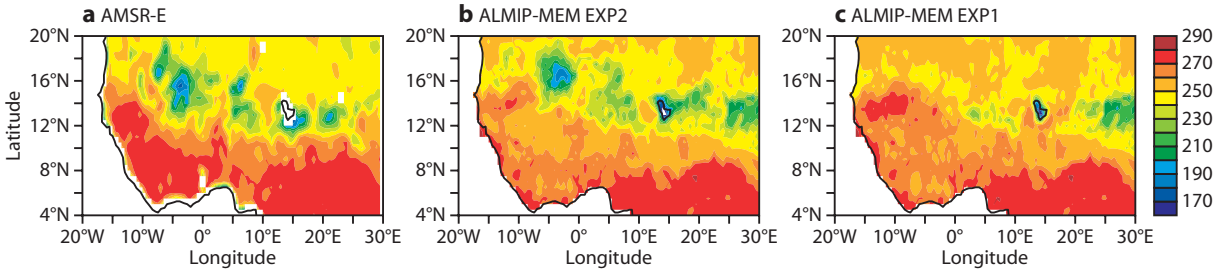

Figure 4: C-band brightness temperature at horizontal polarisation on DoY 200-201: observed by AMSR-E (left), ORCHIDEE simulations in ALMIP-MEM for EXP2 (middle) and EXP1 (right).

the time-latitude diagram of the horizontally polarised brightness temperatures at C-band from AMSR-E and using the ALMIP-MEM EXP2 and the eight LSMs indicated in Table 2.

For each LSM a bias correction has been applied which subtracts the annual-mean value. The time-latitude diagram (Figure 5) shows the simulated brightness temperature evolutions when CMEM is used with the Kirdyashev vegetation opacity model and the Wand and Schmugge dielectric model. The Kirdyashev vegetation opacity model is the best modelling configuration for any of the considered LSMs. AMSR-E C-band data show a wet patch over Sahel during the rainy season, centred at day 210 and latitude 15.5° North. This wet patch is captured by all the LSMs, but the amplitude is either overestimated or underestimated depending on the LSM. However, this figure underlines the general good agreement between the model-based simulations and the satellite data.

Taylor diagrams display the normalised Standard Deviation (SDV) as a radial distance and the correlation between modelled and observed brightness temperatures as an angle in a polar plot. In Figure 6 a) results for the eight LSMs using the same meteorological forcing and one identical CMEM configuration are presented. Figure 6 b) addresses the performances of one LSM (HTESSEL) coupled to different microwave model configurations.

The normalised standard deviations in simulated brightness temperatures for the year 2006 lie in the range of 0.67 to 1.36, and correlation values between modelled and observed brightness temperatures vary between 0.54 and 0.73 (Figure 6 (a)). The scatter for the different LSMs results from differences in land-surface process parameterisations leading to different simulations of soil moisture and soil temperature profiles. In contrast, in Figure 6 (b) one LSM (HTESSEL) is used for several microwave-emission model configurations. The scatter in model performance varies from 1.0 to 1.4 for the SDV and from -0.01 to 0.54 for the correlation. In these simulations, soil moisture and soil temperature profiles are identical, but the parameterisation of the soil dielectric constant and vegetation opacity are different.

The results presented in Figures 6 (a) and (b) clearly show that, in terms of correlation, the scatter due to the microwave emission model is larger than that due to the LSMs. This figure also points out that the Kirdyashev model (numbers 2, 6, 10 in Figure 6 (b) for the Dobson, Mironov and Wang & Schmugge dielectric models respectively) leads to much better performances than the other vegetation opacity models in terms of both SDV and correlation. The scatter due to the soil dielectric constant model is less important than that due to vegetation opacity. Furthermore, it shows that the Wang and Schmugge model provides best results whatever opacity model is used for the vegetation. Results illustrated here with HTESSEL are confirmed for all the ALMIP-MEM LSMs. There is only one LSM (ORCHIDEE) for which the Mironov dielectric model performs slightly better than the Wang and Schmugge model. The robustness of the Kirdyashev vegetation opacity-model

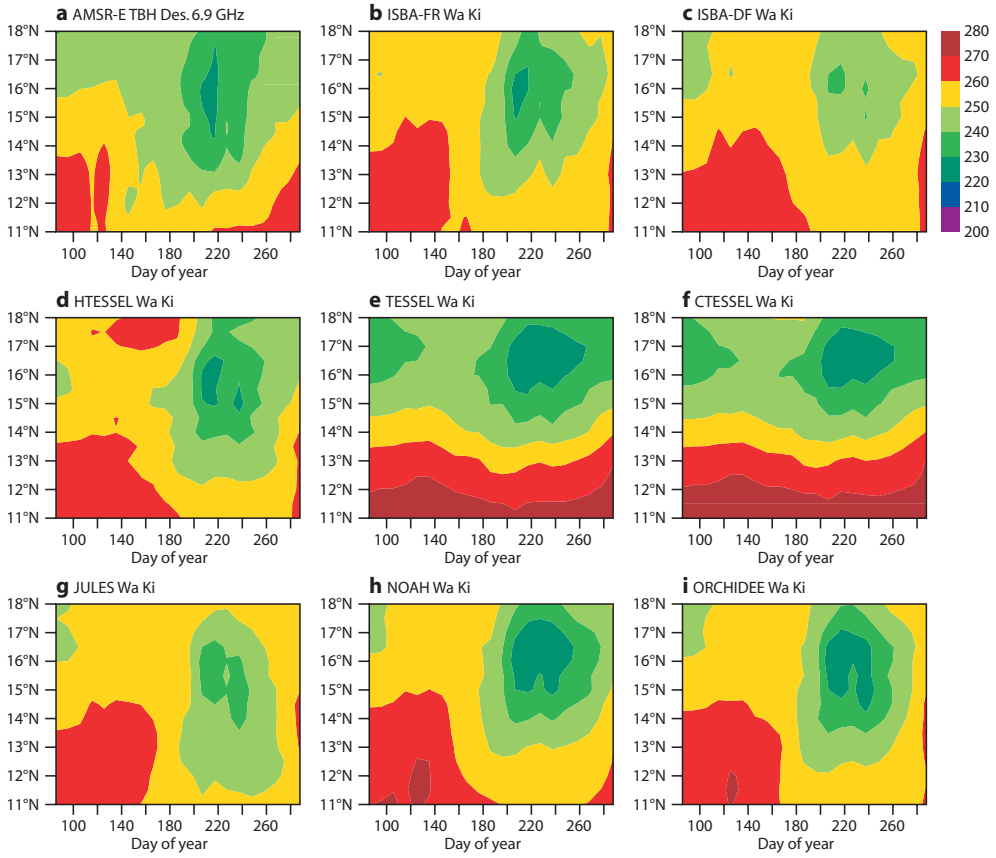

Figure 5: Time-latitude diagram of the horizontally polarised brightness temperature observed by AMSR-E and simulated by ALMIP-MEM for EXP2 (2006). For each ALMIP-MEM simulation a bias correction was applied, specifically computed for each LSM when comparing simulated and observed brightness temperature.

to provide best agreement of simulated brightness temperature for different precipitation forcing and different LSMs is particularly noteworthy.

5 CMEM technical description

5.1 Model coding structure

CMEM is coded in Fortran 90. It is a new highly modular software package providing Input/Output (I/O) interfaces for the Numerical Weather Prediction Community. CMEM was specifically designed to be highly modular in terms of both physics and input/output interface. To reach this modular structure, each component of the microwave emission system and each component of the code are externalized in a separate module. The different subroutines of a module can be interchanged to different I/O format and/or different physical parameterizations. For the user, this allows choosing between different options in the simulation definition without requiring any change on the code.

The CMEM code is organized as described in Figure7, with the main program named cmem_main.F90. Radiative transfer computation of CMEM is modular, it is structured in four modules for soil, vegetation, snow and atmosphere as detailed in Figure 8.

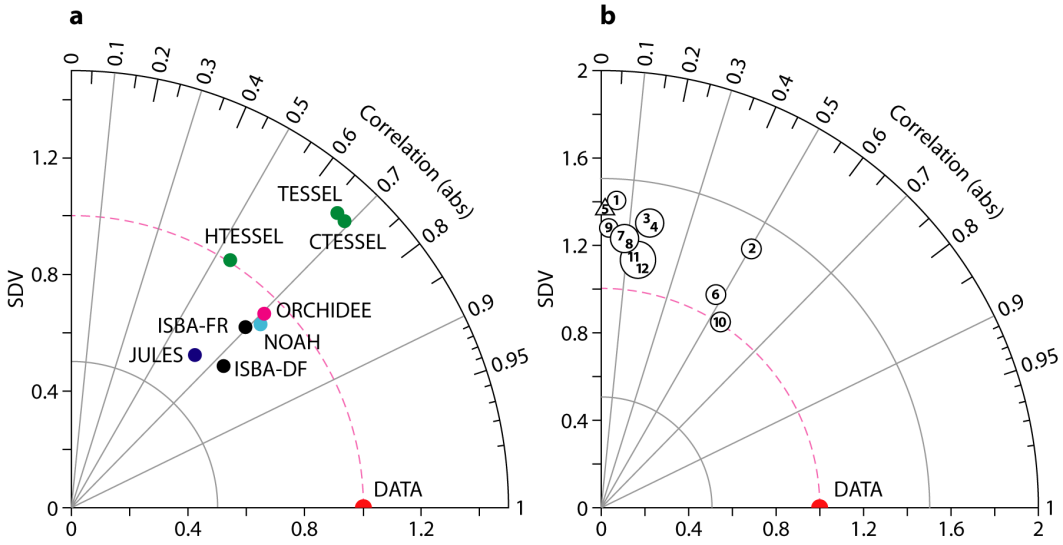

Figure 6: Taylor diagram illustrating the statistics of the comparison between ALMIP-MEM synthetic brightness temperature and AMSR-E data at C-band for (a) different LSMs coupled to CMEM using the Wang and Schmugge dielectric model coupled to the Kirdyashev vegetation opacity model, (b) the HTESSEL LSM coupled to CMEM using different configurations of the microwave emission modelling. The numbers indicated within the circle (right) refer to the vegetation opacity and dielectric models combination obtained from Table 3. Note that the radial axis scale is different for (b).

5.2 Input / Output of CMEM

Figure 9 illustrates the Input/Output structure of CMEM. Four namelist files are provided to CMEM (namdef.h, namopt.h, namrad.h, namlev,h). Setup values are defined in the file named *input*, were the run definition, modular options, observing configuration and soil levels are indicated. The *input* file allows the user to controle the use of CMEM without any need to look into the code itself. It also allows to define the IO configuration by choosing the files formats. Indeed CMEM Input/Output is coded in a modular way, so that the user can choose either ASCII, GRIB or NETCDF I/O format. For any of these I/O type, CMEM is flexible with automatic detection of the Input files sizes. For Grib I/O users can choose tio decode input and encode outoput either with GRIBEX or with the new GRIB API software developed at ECMWF. Both GRIBEX and GRIB API are freely availabale to download fromn the ECMWF web page. Once the *input* file is red to define the simulation configuration and the namelists are red, CMEM scans the input files to get geophysical information as described in the previous section (soil moisture and temperature, vegetation type and fraction, soil texture). CMEM checks the dimensions consistency between the input files, it allocate memory accordingly and then it reads the content of the input files.
Concerning the output of CMEM, the user can choose from the *input* file the output level through the *JPHISTLEV* variable:

- *JPHISTLEV=1*: ouput files contain TBh, TBv, and effective temperature.
- *JPHISTLEV=2*: output files contain all level 1 outputs plus vegetation and atmospheric optical depths, bare soil fraction, atmospheric upward brightness temperature and vegetation water content.
- *JPHISTLEV=3*: output files contain all level 1 and level 2 outputs plus land cover fraction, b parameter, h roughness parameter, as well as horizontal and vertical emissivities.

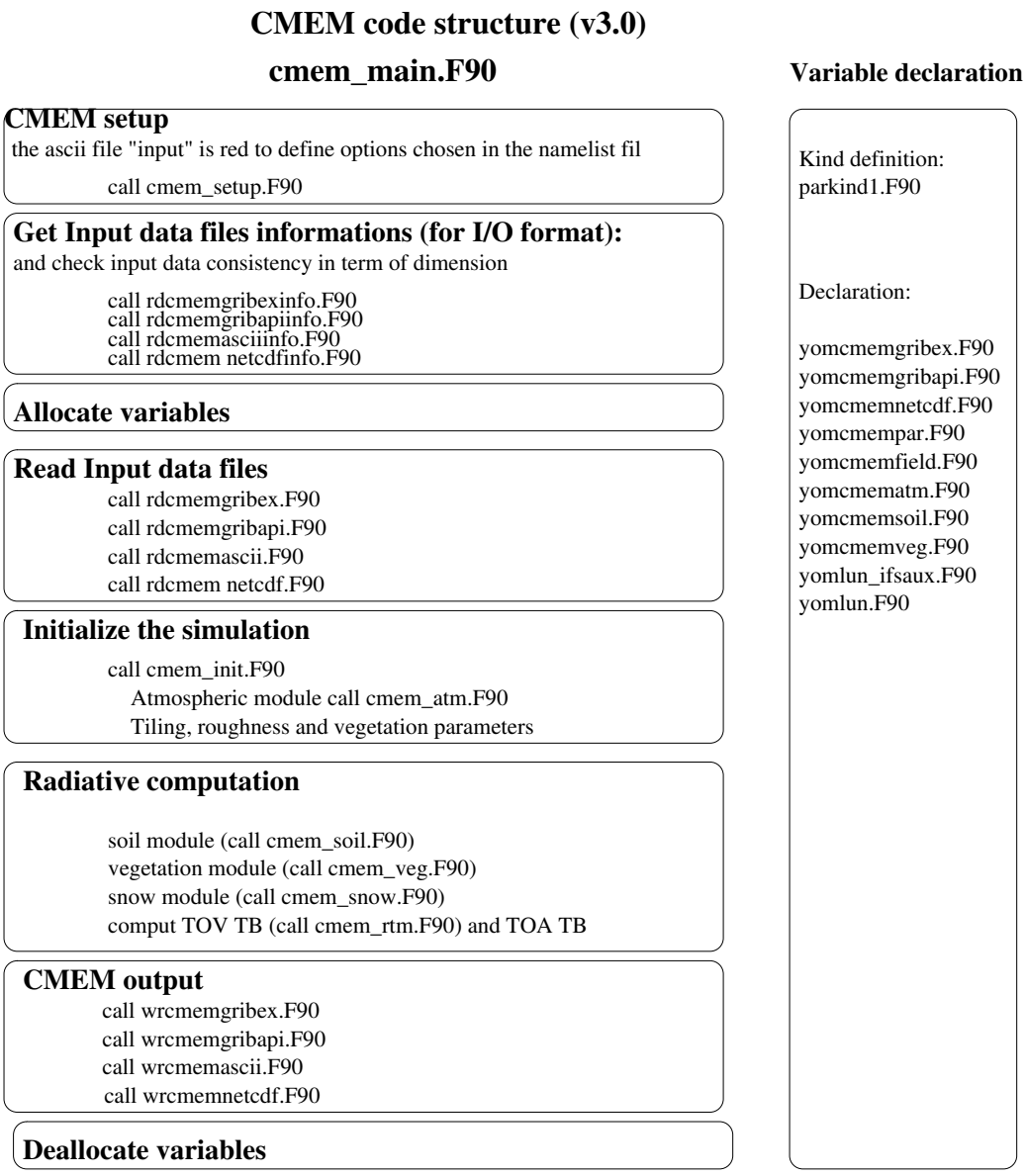

Figure 7: CMEM code Fortran 90 structure.

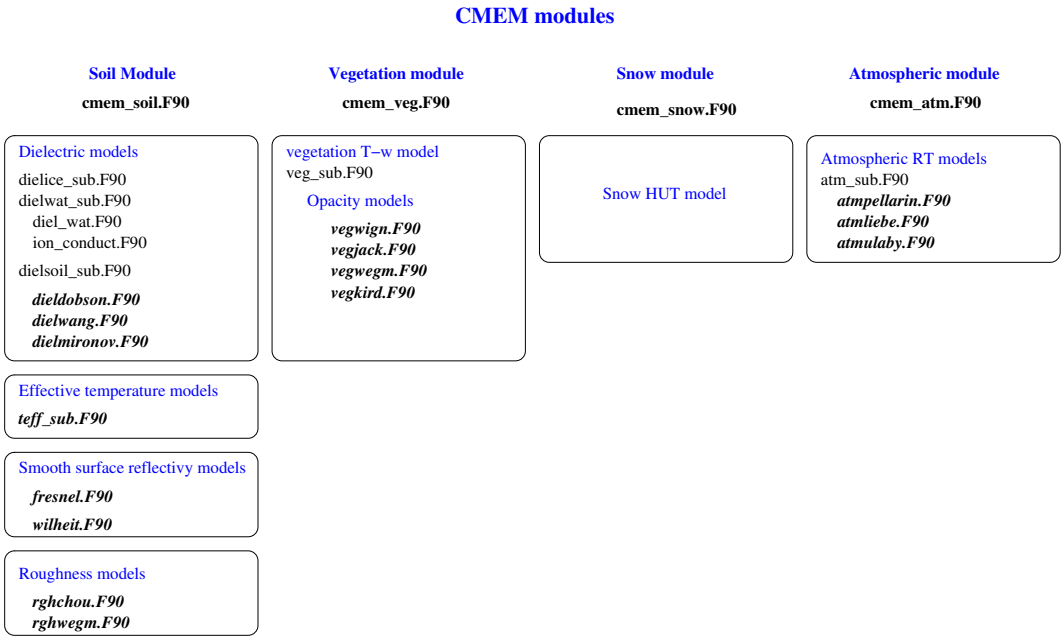

Figure 8: CMEM code modular components.

5.3 CMEM web page and user's interface

ECMWF and ESA agreed to open CMEM sources to the SMOS calibration and validation team members as well as to the entire scientific community. To facilitate the access and the use of CMEM a web page has been set up at ECMWF from which the code of CMEM is available to be downloaded together with a complete technical documentation and readme files: `http://www.ecmwf.int/research/ESA_projects/SMOS/cmem/cmem_index.html`. CMEM's web page is under the ECMWF SMOS web page (Figure 10) that contains information concerning ECMWF activities in SMOS as well as, under a restricted area page, project documents and meeting reports.

CMEM is released through tagged versions. The first tagged version v1.1 has been released in December 2007. The current version in November 2009 is CMEM version 3.0. CMEM's web page includes an up-to-date users list as well as a Frequently Asked Qusetions part.

6 Conclusion

L-band brightness temperatures measured by SMOS are a new observation type which has never been used in NWP applications before. In this report the CMEM observation operator developed by ECMWF is presented and a scientific and technical descriptions are provided. The scientific results, summarised in this report, are based on different observation systems deployed at different times and locations capturing processes at various scales. However, the findings are consistent in that the importance of the forward operator, i.e. the microwave emission model, has been evidenced. In addition, the key parameterisations have been identified and we have shown that the resulting brightness temperatures resemble the main signatures obtained from the corresponding observations. Implementation of CMEM in the IFS will ensure monitoring of SMOS observations from shortly after its launch in 2009, as described in the MS1TN-P2 report.

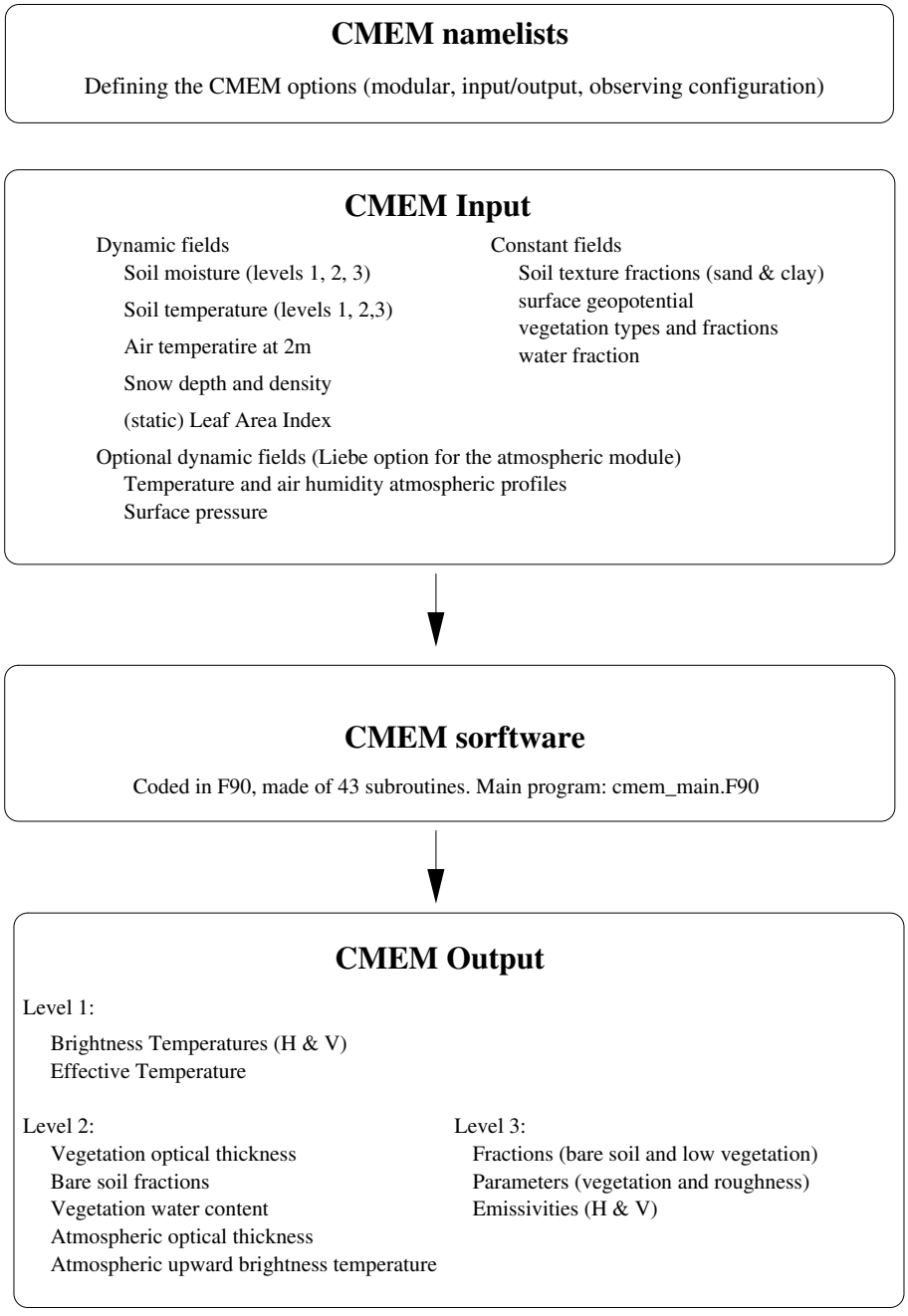

Figure 9: CMEM code modular components.

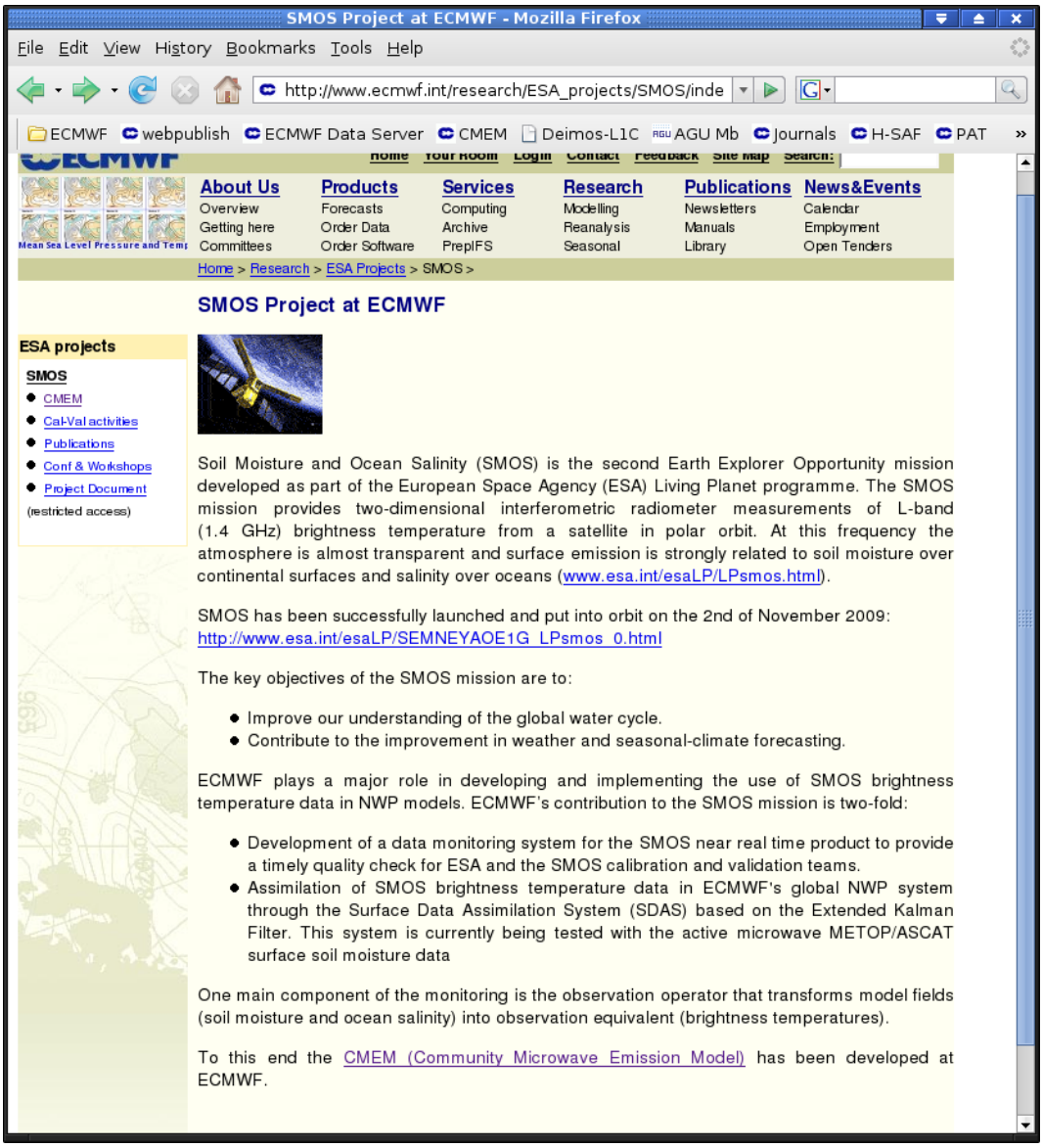

Figure 10: SMOS web page at ECMWF.

Acknowledgements

This work has been funded by the ESA/ESRIN contract number 20244/07/I-LG and is part-1 of Milestone-1 Technical Note (MS1TN-P1). The authors thank Thomas Holmes for his contribution to the initial version of CMEM, as well as Gianpaolo Balsamo for the fruitful interactions we have. We also thank Lars Isaksen, Erik Andersson and Jean-Noël Thépaut for their advice.

References

Balsamo, G., P. Viterbo, A. Beljaars, B. van den Hurk, M. Hirsch, A. Betts, and K. Scipal, 2008: A revised hydrology for the ECMWF model: Verification from field site to terrestrial water storage and impact in the Integrated Forecast System. *ECMWF Tech. Memo. 563; also submitted to Journal of Hydrometeorology*, .

Blyth, E., M. Best, P. Cox, R. Essery, O. Boucher, R. Harding, C. Prentice, P. Vidale, and I. Woodward, 2006: JULES: a new community land surface model. *IGBP Newsletter, October*, .

Boone, A., P. de Rosnay, G. Balsamo, A. Beljaars, F. Chopin, B. Decharme, C. Delire, A. Ducharne, S. Gascoin, F. Guichard, Y. Gusev, P. Harris, L. Jarlan, L. Kergoat, E. Mougin, O. Nasonova, A. Norgaard, T. Orgeval, C. Ottl, I. Poccard-Leclercq, J. Polcher, I. Sandholt, S. Saux-Picart, C. M. Taylor, and Y. Xue, 2009: he AMMA Land Surface Model Intercomparison Project (ALMIP). *IAHS Publ.*, **303**.

Boone, A., and P. de Rosnay, 2007: AMMA forcing data for a better understanding of the West African monsoon surface-atmosphere interactions. Quantification and Reduction of Predictive Uncertainty for Sustainable Water Resource Management. *IAHS Publ.*, **303**.

Boone, A., V. Masson, T. Meyers, and J. Noilhan, 2000: The Influence of the Inclusion of Soil Freezing on Simulations by a SoilVegetationAtmosphere Transfer Scheme. *J. Appl. Meteorol.*, **39(9)**.

Cardona, M., M. Vall-llossera, S. Blanch, A. Camps, A. Monerris, I. Corbella, F. Torres, and N. Duffo, 2005 : Properties of different soil types collected during the mouse 2004 field experiment. *IGARSS 2004, Seoul, Korea*.

Chopin, F., J. Berges, M. Desbois, I. Jobard, and T. Lebel, 2004: Multi-scale precipitation retrieval and validation in african monsoon systems. *2nd International TRMM Science Conf., 6-10 Spet. Nara, Japan*, .

Chen, F., and J. Dudhia, 2001: Coupling an advanced land surface-hydrology model with the Pen State-NCAR MM5 modeling system. Part I: Model implementation and sensitivity. *Mon. Wea. Rev*, **129**.

Choudhury, B., T. Schmugge, A. Chang, and R. Newton, 1979: Effect of surface roughness on the microwave emission from soils. *J. Geophys. Res.*, , 5699–5706.

Choudhury, B., T. Schmugge, and T. Mo, 1982: A parameterization of effective soil temperature for microwave emission. *J. Geophys. Res.*, , 1301–1304.

de Rosnay, P., J.-C. Calvet, Y. H. Kerr, J.-P. Wigneron, F. Lemaître, M.-J. Escorihuela, J. Muñoz Sabater, K. Saleh, J. Barrié, G. Bouhours, L. Coret, G. Cherel, G. Dedieu, R. Durbe, N. Fritz, F. Froissard, J. Hoedjes, A. Kruszewski, F. Lavenu, D. Suquia, and P. Waldteufel, 2006: SMOSREX: A long term field campaign experiment for soil moisture and land surface processes remote sensing. *Remote sensing of Env.*, **102**, pp 377–389; doi:10.1016/j.rse.2006.02.021.

de Rosnay, P., J.-P. Wigneron, T. Holmes, and J.-C. Calvet, 2006 : Parameterizations of the effective temperature for L-band radiometry. Inter-comparison and long term validation with SMOSREX field experiment, Radiative Transfer Models for Microwave Radiometry. *In Mtzler, C., P.W. Rosenkranz, A. Battaglia and J.P. Wigneron (eds.), "Thermal Microwave Radiation - Applications for Remote Sensing", IET Electromagnetic Waves Series 52, London, UK, Christian Matzler (Ed.), Product code: EW 052 ISBN: 0-86341-573-3 and 978-086341-573*.

de Rosnay, P., J. Polcher, M. Bruen, and K. Laval, 2002: Impact of a physically based soil water flow and soil-plant interaction representation for modeling large scale land surface processes. *J. Geophys. Res.*, **107**11.

de Rosnay, P., M. Drusch, A. Boone, G. Balsamo, B. Decharme, P. Harris, Y. Kerr, T. Pellarin, J. Polcher, and J.-P. Wigneron, 2008: Microwave land surface modelling evaluation against amsr-e data over west africa. the amma land surface model intercomparison experiment coupled to the community microwave emission model (ALMIP-MEM). *ECMWF Tech. Memo 576; J. Geophys. Res*, **114**, doi:10.1029/2008JD010724.

Dobson, M., F. Ulaby, M. Hallikainen, and M. El-Rayes, 1985: Microwave dielectric behavior of wet soil-partii: Dielectric mixing models. *IEEE Trans Geosc. Sci*, **38**, 1635–1643.

Drusch, M., T. Holmes, P. de Rosnay, and G. Balsamo, 2009: Comparing ERA-40 based L-band brightness temperatures with Skylab observations: A calibration / validation study using the Community Microwave Emission Model. *ECMWF Tech. Memo 566-2008; and J. Hydrometeo. DOI: 10.1175/2008JHM964.1*, .

Drusch, M., D. Vasilievic, and P. Viterbo, 2004: ECMWF's global snow analysis: Assessment and revision based on satellite observations. *J. Appl. Met.*, **43**, 1282–1294.

Drusch, M., E. Wood, and T. Jackson, 2001: Vegetative and atmospheric corrections for soil moisture retrieval from passive microwave remote sensing data: Results from the Southern Great Plains Hydrology Experiment 1997. *J. Hydromet.*, **2**, 181–192.

Eagleman, J., and W. Lin, 1976: Remote sensing of soil moisture by a 21-cm passive radiometer. *J. Geophys. Res.*, **81**, 3660–3666.

FAO, 2003: Digital soil map of the world (DSMW). Tech. rep. re-issued version.

Holmes, T., P. de Rosnay, R. de Jeu, J.-P. Wigneron, Y. Kerr, J.-C. Calvet, M.-J. Escorihuela, K. Saleh, and F. Lemaître, 2006: A new parameterization of the Effective Temperature for L-band Radiometry. *Geophy. Res. Letters*, **33**, L07405, doi:10.1029/2006GL025724.

Jackson, T. J., A. Y. Hsu, A. V. de Griend, and J. R. Eagleman, 2004: Skylab l-band microwave radiometer observations of soil moisture revisited. *International Journal of Remote Sensing*, **25**, 2585–2606.

Jackson, T., and P. O'Neill, 1990: Attenuation of soil microwave emission by corn and soybeans at 1.4and 5 ghz. *IEEE Trans. Geosc. Remote Sens.*, **28(5)**, 978–980.

Jackson, T., and T. Schmugge, 1991: Vegetation effects on the microwave emission of soils. *Remote sens. environ.*, **36**, 203–212.

Jarlan, L., G. Balsamo, S. Lafont, A. Beljaars, J.-C. Calvet, and E. Mougin, 2007: Analysis of Leaf Area Index in the ECMWF land surface scheme and impact on latent heat and carbon fluxes: Applications to West Africa. Tech. rep.

Kerr, Y., 2007: Soil Moisture from space: Where we are ? *Hydrogeology journal*, **15**, 117–120.

Kerr, Y., P. Waldteufel, J.-P. Wigneron, J.-M. Martinuzzi, J. Font, and M. Berger, 2001: Soil moisture retrieval from space: The soil moisture and ocean salinity (smos) mission. *IEEE Trans. Geosc. Remote Sens.*, **39 (8)**, 1729–1735.

Kirdyashev, K., A. Chukhlantsev, and A. Shutko, 1979: Microwave radiation of the earths surface in the presence of vegetation cover. *Radiotekhnika i Elektronika*, **24**, 256–264.

Klein, L.A. and C.T. swift, 1977: An improved model for the dielectric constant of sea water at microwave frequencies, *IEEE Trans. Antennas Prop.*, **25 (1)**, 104–111.

Liebe, H., 2004: MPM- An atmospheric millimeter-wave propagation model. *Int. J. Infrared Millimeter Waves*, **10**, 631–650.

Masson, V., J.-L. Champeaux, F. Chauvin, C. Meriguet, and R. Lacaze, 2003: A global database of land surface parameters at 1-km resolution in meteorological and climate models. *J. Climate*, **97(1r61)**, 1261–1282.

Mironov, V., M. Dobson, V. Kaupp, S. Komarov, and V. Kleshchenko, 2004: Generalized refractive Mixing dielectric model for moist soils. *Soil Sci. Soc. Am. J.*, **42(4)**, 773–785.

Njoku, E., 2004: updated daily. AMSR-E/AQUA daily L3 surface soil moisture, interpretive parms, & QC EASE-Grids. *Boulder, CO, USA: National Snow and Ice Data Center*, **Digital Media**.

Njoku, E., T. Jackson, V. Lakshmi, T. Chan, and S. Nghiem, 2003: Soil moisture retrieval from AMSR-E. *IEEE Trans. Geosc. Remote Sens.*, **41(2)**, 215–229.

Noilhan, J., and S. Planton, 1989: A simple parameterization of land-surface processes for meteorological models. *Mon. Wea. Rev.*, **117**, 536–549.

Pellarin, T., J.-P. Wigneron, J.-C. Calvet, M. Berger, H. Douville, P. Ferrazzoli, Y. Kerr, E. Lopez-Baeza, J. Pulliainen, L. Simmonds, and P. Waldteufel, 2002: Two-year global simulation of L-band brightness temperature over land. *IEEE Trans. Geosc. Remote Sens.*, **41(4)**, 2135–2139.

Pulliainen, J., M. Hallikainen, and J. Grandell, 1999: HUT snow emission model and its applicability to snow water equivalent retrieval. *IEEE Trans. Geos. Remot. Sens*, **37**, 1378–1390.

Redelsperger, J.-L., C. Thorncroft, A. Diedhiou, T. Lebel, D. Parker, and J. Polcher, 2006: African Monsoon, Multidisciplinary Analysis (AMMA): An International Research Project and Field Campaign. *Bull. Amer. Meteorol. Soc*, **87(12)**, 1739–1746.

Sabater Muñoz, J. P. de Rosnay and G. Balsamo, 2009: Sensitivity of L-band NWP forward modelling to soil roughness. *International Journal of Remote Sensing* , **submitted**.

Saunders, R., M. Matricardi, and P. Brunel, 1999: An improved fast radiative transfer model for assimilation of satellite radiance observations. *Quart. J. Roy. Met. Soc.*, **125**, 1407–1425.

SMOS ATBD, 2007: SMOS Expert Support Laboratories, SMOS level 2 Processor for Soil Moisture Algorithm Theoretical Based Document (ATBD). *SO-TN-ESL-SM-GS-0001, issue 2.a*, , 124.

Ulaby, F., R. Moore, and A. Fung. *Microwave remote sensing: active and passive, Vol III, from theory to application*. Artech House, Dedham, MA, 1986.

Uppala, S., and . co authors, 2005: The ERA-40 re-analysis. *Quart. J. Roy. Meteorol. Soc.*, **131**, 2961–3012.

Viterbo, P., and A. C. M. Beljaars, 1995: An improved land surface parametrization scheme in the ECMWF model and its validation. *ECMWF Tech. Report No. 75*, . Research Department, ECMWF.

Wang, J. & T. Schmugge, 1980: An empirical model for the complex dielectric permittivity of soils as a function of water content. *IEEE Trans. Geosc. Remote Sens.*, **18**, 288–295.

Wang, J.R. and B.J. Choudhury, 1981: Remote sensing of soil moisture content over bare field at 1.4 GHz frequency, *J. Geophys. Res.*, **86**, 5277–5282.

Wegmüller, U. & C. Mätzler, 1999: Rough bare soil reflectivity model. *IEEE Transactions on Geoscience Electronics*, **37**, 1391–1395.

Wegmüller, U., C. Mätzler, and E. Njoku, 1995: Canopy opacity models, in passive microwave remote sensing of land-atmosphere interactions. *B. et al. Ed. Utrecht, The Netherlands: VSP*, , 375.

Wigneron, J.-P., Y. Kerr, P. Waldteufel, K. Saleh, M.-J. Escorihuela, P. Richaume, P. Ferrazzoli, P. de Rosnay, R. Gurney, J.-C. Calvet, M. Guglielmetti, B. Hornbuckle, C. Mätzler, T. Pellarin, and M. Schwank, 2007: L-band Microwave Emission of the Biosphere (L-MEB) Model: description and calibration against experimental data sets over crop fields. *Remote sens. environ.*, **107**, 639–655.

Wigneron, J.-P., L. Laguerre, and Y. Kerr, 2001: A Simple Parmeterization of the L-band Microwave Emission from Rough Agricultural Soils. *IEEE Trans. Geosc. Remote Sens.*, **39**, 1697–1707.

Wilheit, T., 1978: Radiative transfert in plane stratified dielectric. *IEEE Transactions on Geoscience Electronics*, **16(2)**, 138–143.